those of the enzyme BESOD.

The potential of the reduction is not strongly dependent upon solvent, indicating that the initial and reduced species are interacting with the solvent in a similar manner. The reoxidation wave depends on many variables, however. Its solvent dependence shows that one of the species involved in this redox process interacts more strongly with the solvent than does the other. Reoxidation of the unbridged complex in the presence of 1 equiv of added 1-methylimidazole is similar to reoxidation of the bridged species. Moreover, the relative current of the reoxidation increases upon addition of water. These results suggest that the complex being reoxidized following reduction of $[Cu_2(im)\subset A']^{3+}$ might be a species with the imidazolate bridge broken.

**Comparisons with BESOD.** The original purpose for synthesizing imidazolate-bridged complexes was to study them as models for the active site of the enzyme BESOD.[1] The first discrete imidazolate-bridged complexes, using bpim as the source of imidazolate,[3] had magnetic and structural properties different from those of the four-copper form of the enzyme.[16] The next generation of imidazolate-bridged complexes, using simple tridentate ligands for the copper and imidazolate, had magnetic properties similar to those of the enzyme, but the imiidazolate bridge was never 100% intact in solution and was only a major species in solution over a narrow pH range.[2] The macrocycles provide a very stable environment for the $Cu_2(im)^{3+}$ ion. It remains intact over a wide pH range, exhibiting a stability similar to that of the imidazolate bridge in the enzyme. The magnetic properties of $[Cu_2im(imH)_2\subset A]^{3+}$ and $[Cu_2im\subset A']^{3+}$ also match those of $Cu_2Cu_2SOD$.

The form of the enzyme with copper in the copper site and nothing in the zinc site, $Cu_2E_2BESOD$, has an unusual pH-dependent metal migration[27] for which some of the chemistry reported here is a good model. At neutral pH the ESR spectrum of $Cu_2E_2SOD$ resembles that of mononuclear copper, as expected since each copper ion is in a separate subunit. As the pH is raised, the ESR spectrum changes from that of mononuclear copper to a spectrum similar to that of $Cu_2Cu_2SOD$. The copper ions migrate to form an imidazolate-bridged dicopper(II) unit in a single subunit. This behavior was also observed in solutions of copper:macrocycle:imidazole in 1:1:1 ratios.

One area in which the macrocyclic complex is less satisfactory as a model for BESOD or $Cu_2Cu_2SOD$ involves the redox chemistry of the copper ions. The redox potential of the copper in native BESOD is much more positive than the potential in the macrocyclic complex. The high redox potential of the enzyme is probably due to the tetrahedral distortion of the copper site revealed in the high-resolution X-ray crystal structure of BESOD.[28] Additional comparisons of the properties of $[Cu_2(im)\subset A]^{3+}$ and $[Cu_2(im)\subset A']^{3+}$ with those of superoxide dismutase and its derivatives are given elsewhere.[1]

**Acknowledgment.** This work was supported by research grants from the National Science Foundation and the National Institute of General Medical Sciences, NIH. We thank J. V. Plust for technical assistance. We also thank Drs. A. E. Martin and J. Bulkowski for providing a generous amount of the ligand A'.

**Registry No.** $[Cu_2(im)(imH)_2\subset A](ClO_4)_3$, 69470-57-1; $[Cu_2(im)\subset A'](ClO_4)_3$, 76096-70-3; $[Cu_2(im)(imH)_2\subset A]^{3+}$, 69470-56-0; $[Cu_2(im)\subset A']^{3+}$, 76096-69-0.

**Supplementary Material Available:** Tables S1 and S2 listing observed and calculated molar susceptibilities and magnetic moments vs. temperature for $[Cu_2(im)(imH)_2\subset A](ClO_4)_3$ and $[Cu_2(im)\subset A'](ClO_4)_3\cdot H_2O$, respectively (5 pages). Ordering information is given on any current masthead page.

(27) Valentine, J. S.; Pantoliano, M. W.; McDonnell, P. J.; Burger, A. R.; Lippard, S. J. *Proc. Natl. Acad. Sci. U.S.A.* **1979**, *76*, 4245.

(28) Tainer, J. A.; Getzoff, E. D.; Beem, K. M.; Richardson, J. S.; Richardson, D. C. *J. Mol. Biol.* **1982**, *160*, 181.

Contribution from the Department of Chemistry, University of Houston, Houston, Texas 77004

# Electron-Transfer and Ligand-Addition Reactions of (TPP)Mn(NO) and (TPP)Co(NO) in Nonaqueous Media

S. KELLY, D. LANÇON, and K. M. KADISH*

*Received September 19, 1983*

The electron-transfer and ligand-addition reactions of the manganese and cobalt porphyrin complexes (TPP)Mn(NO) and (TPP)Co(NO) were studied in nine nonaqueous solvents. In all solvents, stable complexes of $[(TPP)Co(NO)]^-$, $[(TPP)Co(NO)]^+$, $[(TPP)Mn(NO)]^-$, and $[(TPP)Mn(NO)]^{2-}$ could be generated at the electrode surface. In contrast, $[(TPP)Mn(NO)]^+$ was not stable and rapidly decomposed to yield $[(TPP)Mn]^+$ and NO. Spectrophotometric and electrochemical studies in mixed-solvent systems provide clear evidence for the presence of $[(TPP)Co(NO)(L)]^+$ and (TPP)Mn(NO)(L) in solution, where L = DMF, $Me_2SO$, and pyridine, and stepwise formation constants for the addition of these ligands are determined. Finally, comparisons are made between the electrochemical stability of (TPP)M(NO) and the metal-nitrosyl bond where M = Cr(II), Mn(II), Fe(II), and Co(II).

## Introduction

The reactions of nitric oxide with synthetic metalloporphyrin complexes containing divalent transition metals have been extensively investigated in the last 10 years. Many of these studies have concentrated on Fe(II) porphyrins[1-9] while nitrosyl complexes with metalloporphyrins containing central metals other than iron have received less attention in the literature. The nitrosyl complexes of synthetic manganese and chromium

(1) Wayland, B. B.; Olson, L. W. *J. Am. Chem. Soc.* **1974**, *96*, 6037.
(2) Scheidt, W. R.; Frisse, M. E. *J. Am. Chem. Soc.* **1975**, *97*, 17.
(3) Scheidt, W. R.; Piciulo, P. L. *J. Am. Chem. Soc.* **1976**, *98*, 1913.
(4) Buchler, J. W.; Lay, K. L. *Z. Naturforsch., Anorg. Chem., Org. Chem.* **1975**, *30*, 385.
(5) Yoshimura, T. *Arch. Biochem. Biophys.* **1982**, *216*, 625.
(6) Yamamoto, T.; Nozawa, T.; Kaito, A.; Hatano, M. *Bull. Chem. Soc. Jpn.* **1982**, *55*, 2021.
(7) Wayland, B. B.; Minkiewicz, J. V.; Abd-Elmageed, M. E. *J. Am. Chem. Soc.* **1974**, *96*, 2795.
(8) Olson, L. W.; Schaeper, D.; Lançon, D.; Kadish, K. M. *J. Am. Chem. Soc.* **1982**, *104*, 2042.
(9) Lançon, D.; Kadish, K. M. *J. Am. Chem. Soc.* **1983**, *105*, 5610.

0020-1669/84/1323-1451$01.50/0 

porphyrins have been characterized via ESR, electronic absorption spectra, and IR spectroscopy,[10,11] and the crystallographic structure of (TPP)Mn(NO)(4-MePip) has been determined.[12] Other nitrosylated metalloporphyrin complexes that have been identified and characterized include those of ruthenium[13] and rhodium.[14]

Wayland et al.[7] spectroscopically investigated the binding of NO and other diatomic ligands to (TPP)Co and, on the basis of these data, designed a bonding model for Co(II) and Fe(II) porphyrins with CO, $O_2$, and NO. Crystallographic studies on nitrosyl complexes of Mn(II),[12] Fe(II),[2,3,12] and Co(II)[15] porphyrins have shown that the M–N–O bond angle depends greatly upon the central metal. This agrees with molecular orbital calculations[16–19] that predict significant changes in the nature of the metal–nitrosyl bond with changes in the number of metal d electrons.

Our own laboratory has been interested in characterizing the electrochemical properties of transition-metal porphyrins complexed by nitric oxide. In initial papers we have concentrated on the electrode reactions of $PFe(NO)$,[8,9] $PFe(NO)_2$,[8,9] and $PCr(NO)$[20] where P = $TPP^{2-}$ or $OEP^{2-}$. In this paper we extend these studies to complexes of (TPP)Mn(NO) and (TPP)Co(NO). We have characterized the electron-transfer and ligand-binding reactions of (TPP)Mn(NO) and (TPP)Co(NO) in a number of solvents and have compared our results to those obtained for (TPP)Fe(NO) and (TPP)Cr(NO) in the nonbonding solvent $CH_2Cl_2$. By virtue of this comparison, the influence of metal d electrons on a number of (TPP)M(NO) characteristics can be better understood. The characteristics that we have considered in this paper include the effect of nitrosylation upon the stability of each metal oxidation state, the effect of solvent on the various redox reactions of (TPP)M(NO), and the magnitude of formation constants for the axial addition of a donor base to (TPP)M(NO) or to one of the oxidized or reduced nitrosylated complexes.

## Experimental Section

**Chemicals.** (TPP)Mn(NO) was synthesized via published methods[11] from (TPP)MnCl. This latter compound was synthesized from $TPPH_2$ and $Mn(OAc)_2$ (Fisher Scientific) by using published procedures.[21] Free-base *meso*-tetraphenylporphyrin was synthesized by the method of Adler et al.,[22] with chlorin impurities removed by the method of Rosseau and Dolphin.[23] (TPP)Co(NO) was synthesized from (TPP)Co via the method of Wayland et at.[7] (TPP)Co was obtained from Strem Chemical Co. and used without further purification.

Nine nonaqueous, aprotic solvents were used in this study. Their suppliers and methods of purification have recently been published.[20] Nitric oxide was purchased from Union Carbide Co. and was passed through a dry ice–acetone bath and over KOH pellets before use to remove higher oxides of nitrogen. All solutions contained 0.1 M TBAP, which was purchased from Eastman Kodak Co. and recrystallized from ethanol before use. Ferrocene was purchased from Aldrich Chemical Co. and was purified by vacuum sublimation.

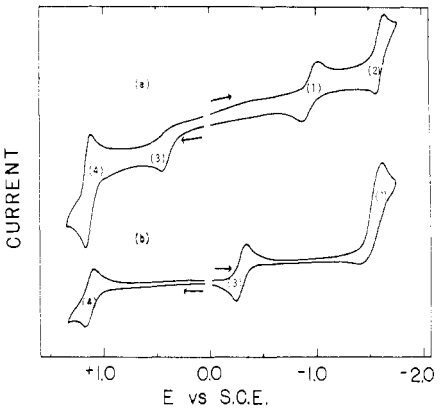


**Figure 1.** Cyclic voltammograms in $CH_2Cl_2$/0.1 M TBAP solutions: (a) $10^{-3}$ M (TPP)Mn(NO); (b) $10^{-3}$ M (TPP)MnCl.

**Instrumentation.** Voltammetric measurements were obtained by using one of three different experimental setups. For measurements at slow scan rates, either a PAR Model 174A polarographic analyzer or an IBM Model 225A voltammetric analyzer was used in conjunction with an Omnigraphic 2000 X-Y recorder. Scan rates faster than 200 mV/s were obtained with use of a PAR Model 173 potentiostat/galvanostat and a PAR Model 178 electrometer probe driven by either a PAR Model 175 universal programmer or a Hewlett-Packard Model 3310 B function generator. Current–voltage curves, which were taken at sweep rates between 0.50 and 50.0 V/s, were recorded on a Tektronix Model 5111 storage oscilloscope with a Tektronix Model C-5A camera attachment.

*iR* loss at high scan rates was held to a minimum by use of positive feedback devices built into both the IBM Model 225A and the PAR Model 176 current follower plug-in (which is used with the PAR Model 173 potentiostat). The appropriate amount of *iR* compensation was determined by dialing the 10-turn pot on the plug-in until the operational amplifier was set into oscillation. At this point, the pot was reversed just enough to end the oscillation. This procedure was repeated each time the potential sweep rate was altered.

All three instrument setups for voltammetric measurements used a three-electrode configuration, consisting of a platinum-button working electrode, a platinum counterelectrode, and a saturated calomel reference electrode (SCE). For all experiments the reference electrode was separated from the bulk of the solution by a fritted-glass or a cracked-glass bridge filled with appropriate solvent and supporting electrolyte. The solution in the bridge was changed periodically to prevent aqueous contamination of the cell solution by the reference electrode. Deaeration of all solutions was accomplished by passing a stream of high-purity nitrogen or argon through the solution for 10 min and maintaining a blanket of inert gas over the solution while making the measurements. The inert gas was saturated with the appropriate solvent before entering the cell to minimize the evaporation of solvent from the cell.

Controlled-potential electrolyses were done with the PAR Model 173 potentiostat/galvanostat equipped with a PAR Model 179 digital coulometer plug-in. Coulomb vs. time curves were obtained with a Sargent Model SRLG strip chart recorder. A conventional three-electrode configuration was used in all electrolyses experiments. The platinum-wire-mesh counterelectrode was separated from the bulk of the solution with a type-F sintered-glass frit.

UV-visible spectroscopic measurements were made with either a Cary Model 14 or a Beckman Model 26 spectrophotometer. Thin-layer spectroelectrochemical measurements were performed with either a PAR Model 174A polarographic analyzer or a PAR Model 173 potentiostat/galavanostat coupled to a Tracor Northern 1710 holographic optical spectrometer/multichannel analyzer to obtain time-resolved spectral data. The resulting spectra were recorded on floppy disks using a Data Systems Design Model 440 flexible disk system and a Teletype Corp. Model 43 teleprinter. The thin-layer cell consisted of a 100 lpi gold minigrid sandwiched between two glass slides and assembled in a solution reservoir with counter- and reference electrodes in a manner described by Rhodes and Kadish.[24] The volume

(10) Wayland, B. B.; Olson, L. W. *Inorg. Chim. Acta* **1974**, *11*, 623.
(11) Wayland, B. B.; Olson, L. W.; Siddiqui, Z. V. *J. Am. Chem. Soc.* **1976**, *98*, 94.
(12) Piciulo, P. L.; Rupprecht, G.; Scheidt, W. R. *J. Am. Chem. Soc.* **1974**, *96*, 5293.
(13) Srivastava, T. S.; Hoffman, L.; Tsutsui, M. *J. Am. Chem. Soc.* **1972**, *94*, 1385.
(14) Wayland, B. B.; Newman, A. R. *Inorg. Chem.* **1981**, *20*, 3093.
(15) Scheidt, W. R.; Hoard, J. L. *J. Am. Chem. Soc.* **1973**, *95*, 8281.
(16) Pierpont, C. G.; Eisenberg, R. *J. Am. Chem. Soc.* **1971**, *93*, 4905.
(17) Mingos, D. M. P. *Inorg. Chem.* **1973**, *12*, 1209.
(18) Enemark, J. H.; Feltham, R. D. *Coord. Chem. Rev.* **1974**, *13*, 339.
(19) Elian, M.; Chen, M. M. L.; Mingos, D. M. P.; Hoffman, R. *Inorg. Chem.* **1976**, *15*, 1148.
(20) Kelly, S. K.; Kadish, K. M. *Inorg. Chem.* **1984**, *23*, 679.
(21) Jones, R. D.; Summerville, D. A.; Basolo, F. *J. Am. Chem. Soc.* **1978**, *100*, 4416.
(22) Adler, A. D.; Longo, F. R.; Finarelli, J. D.; Goldmacher, J.; Assour, J. Korsakoff, L. *J. Org. Chem.* **1967**, *32*, 476.
(23) Rosseau, K.; Dolphin, D. *Tetrahedron Lett.* **1974**, *48*, 4251.
(24) Rhodes, R. K.; Kadish, K. M. *Anal. Chem.* **1981**, *53*, 1539.

and path length (~0.1 mm) of the thin-layer cells were calibrated from coulometry using a standard $K_3Fe(CN)_6$ solution. Spectra were typically taken at metalloporphyrin concentrations of 0.1 mM. Because of high solution resistance inherent to the cell design, the supporting electrolyte concentration ranged from 0.5 M in solvents of low dielectric constants to 0.2 M in solvents of high dielectric constants. For thin-layer experiments, potential scan rates of 2 mV/s were typical.

## Results and Dicussion

**Redox Reactions of (TPP)Mn(NO) in $CH_2Cl_2$.** (TPP)Mn(NO) exhibits one irreversible and four reversible redox processes at a Pt electrode in the range of +1.60 to −1.80 V vs. SCE. Four of these reactions are shown in Figure 1a, which illustrates a cyclic voltammogram between +1.2 and −1.8 V vs. SCE. The two most positive electrode reactions are at +1.18 and +1.58 V. An irreversible oxidation is observed at $E_p$ = +0.48 V (at a scan rate of 0.2 V/s), while reversible reductions for this compound are observed at −0.92 and −1.60 V vs. SCE. These latter two reductions appear not to involve loss of nitrosyl, so that the reactions may be described as

$$(TPP)Mn(NO) + e^- \rightleftarrows [(TPP)Mn(NO)]^- \quad (1)$$

$$[(TPP)Mn(NO)]^- + e^- \rightleftarrows [(TPP)Mn(NO)]^{2-} \quad (2)$$

Under the same experimental conditions, (TPP)MnCl exhibits four redox reactions, of which three are shown in Figure 1b. This complex has been characterized as undergoing up to three reductions and two oxidations, depending on the solvent potential range.[25] For (TPP)MnCl, one observes a Mn(III) ⇄ Mn(II) reduction (at −0.29 V), an irreversible ring reduction (at −1.60 V), and two ring oxidations (at +1.18 and +1.58 V). A second ring reduction of (TPP)MnCl is not observed in $CH_2Cl_2$, but this does occur in other solvents. It is interesting to note that the two oxidations and the second reduction of (TPP)MnCl occur at potentials virtually identical with those measured for (TPP)Mn(NO) in $CH_2Cl_2$. For the reduction this similarity in half-wave potentials is only coincidental and, as will be shown later, large potential differences do exist in other solvent systems.

The data in Figure 1 provides strong evidence for stabilization of the Mn(II) oxidation state with respect to Mn(III) in (TPP)Mn(NO). As seen in this figure, the oxidation off (TPP)Mn(NO) is shifted by at least 620 mV[26] from that of (TPP)Mn to yield (TPP)MnX where X = $ClO_4^-$ (the actual observed reaction in this case is the Mn(III) ⇄ Mn(II) reduction). When compared to other forms of (TPP)MnX in $CH_2Cl_2$ (where X = $I^-$, $SCN^-$, $Cl^-$, $Br^-$, or $N_3^-$),[25] this potential stabilization appears to be even greater. For example, for (TPP)$MnN_3$ the Mn(III)/Mn(II) reaction occurs at −0.34 V, which is 820 mV negative of the Mn(II)/Mn(III) reaction for (TPP)Mn(NO) ($E_p$ = +0.480 V).

A large potential shift is also observed for reduction of (TPP)Mn(NO) (reaction 1, Figure 1a) when compared to reduction of the unnitrosylated $[(TPP)MnCl]^-$ species (peak 1, Figure 1b). This 680-mV positive shift for reduction of the Mn(II) complex implies a substantial stabilization of (TPP)Mn(NO) toward reduction and also provides evidence that NO dissociation does not occur upon reduction of (TPP)Mn(NO). Significant shifts in potential are also observed between the reduction of $[(TPP)Mn(NO)]^-$ (reaction 2, Figure 1a) and $[(TPP)MnCl]^-$ (not shown in Figure 1b). These shifts depend largely on the solvent (Table I, ref 25 and 28). In

Table I. Potentials (V vs. SCE) for the Electrode Reactions of (TPP)Mn(NO) in Selected Solvents

| solvent | oxidn $E_p(3)^a$ | redn $E_{1/2}(1)$ | redn $E_{1/2}(2)$ | $E_{1/2}(Fc^+/Fc)$ |
|---|---|---|---|---|
| $CH_2Cl_2$ | 0.48 | −0.92 | −1.60 | 0.49 |
| PhCN | 0.53 | −0.95 | −1.63 | 0.49 |
| *n*-PrCN | 0.51 | −0.99 | −1.62 | 0.46 |
| DMF | 0.55 | −1.01 | −1.55 | 0.50 |
| DMA | 0.60 | −0.98 | −1.52 | 0.55 |
| $Me_2SO$ | 0.58 | −1.00 | −1.48 | 0.46 |
| py | 0.54 | −1.23 | −1.57 | 0.54 |

[a] This reaction is irreversible in all solvents, and potentials quoted are for $E_{pa}$ at 200 mV/s.

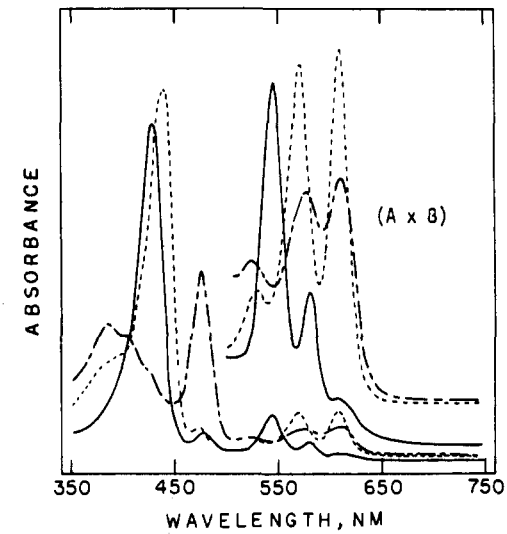


**Figure 2.** Electronic absorption spectra of $10^{-4}$ M (TPP)Mn(NO) in $CH_2Cl_2$/0.1 M TBAP solution, obtained during bulk coulometric experiments: before electrolysis (—); after oxidation at +1.1 V (— — —); rereduction at −0.8 V (- - -).

$Me_2SO$ the shift in $E_{1/2}$ amounts to 210 mV while the potential difference is only 80 mV in $CH_2Cl_2$. Both shifts are in a direction consistent with stabilization of the $[(TPP)Mn(NO)]^{2-}$ products; these values provide further evidence of the Fe–NO bond strength, and that NO is not displaced by binding solvents upon reduction of the $[(TPP)Mn(NO)]^-$ anion.

**Oxidation of (TPP)Mn(NO).** The electrode reactions of (TPP)Mn(NO) were studied in a variety of nonaqueous solvents. A list of the solvents utilized and a summary of the half-wave potentials are given in Table I. The first oxidation of (TPP)Mn(NO) is irreversible in all solvents studied, with $E_{pa}$ = +0.48 V vs. SCE at a scan rate of 200 mV/s in $CH_2Cl_2$/0.1 M TBAP. The second and third oxidations of (TPP)Mn(NO) are reversible and are at potentials comparable to the first two oxidations of (TPP)$MnClO_4$[25] or (TPP)MnCl. These potentials are not shown in Table I since they give no additional information regarding the oxidized forms of (TPP)Mn(NO).

If the first oxidation of (TPP)Mn(NO) involved loss of bound NO after electron transfer, then it would be expected that the oxidation product of (TPP)Mn(NO) and (TPP)MnCl would have similar potentials for any further oxidations. We suggest that this does occur and that peak 4 of (TPP)Mn(NO) and peak 4 of (TPP)MnCl (parts a and b, respectively, of Figure 1) correspond to oxidation of identical species at the electrode surface. In this case, the reacting species would be $[(TPP)Mn]^+$ (or (TPP)$MnClO_4$), which is generated at the electrode surface after a reversible (rapid) oxidation of (TPP)Mn(NO) as shown in (3).

Bulk controlled-potential electrolysis and thin-layer spectroelectrochemical experiments were carried out to characterize

(25) Kelly, S. L.; Kadish, K. M. *Inorg. Chem.* **1982**, *21*, 3631.
(26) Because of the chemical reaction following the reversible electron transfer, the oxidation peak is shifted in a cathodic direction. The magnitude of this shift is governed by the rate constant of the chemical reaction,[27] which in this specific instance is too fast to measure by cyclic voltammetric techniques.
(27) Nicholson, R. S.; Shain, I. *Anal. Chem.* **1964**, *36*, 706.
(28) Kadish, K. M.; Morrison, M. M. *Bioelectrochem. Bioenerg.* **1976**, *3*, 480.

$$(TPP)Mn(NO) \xrightarrow{-e^-} [(TPP)Mn(NO)]^+ \rightarrow [(TPP)Mn]^+ + NO \quad (3)$$

the products of reaction 3. The results of this oxidation and rereduction are shown in Figure 2. Abstraction of 1.0 electrons from (TPP)Mn(NO) produces a species whose UV–visible absorption spectrum does not resemble that published for (TPP)Mn(NO)X,[11] but rather resembles that of (TPP)MnX.[29] Furthermore, rereduction of the oxidized product did not generate the starting spectrum of (TPP)Mn(NO), but rather gave the spectrum of (TPP)Mn.[30] In addition, further oxidation/reduction cycles of the coulometrically oxidized solution produced no evidence for the presence of nitrosyl complexes in solution, and only the spectra of (TPP)MnX and (TPP)Mn were observed. Thus, one can conclude that although (TPP)Mn(NO)X is reportedly stable in toluene at zero ionic strength,[11] it does not appear to be stable in $CH_2Cl_2$ solutions containing 0.1 M TBAP. In fact, none of the eight utilized nonaqueous solvents showed reversible behavior for the first oxidation of (TPP)Mn(NO) (see later sections).

Proof of the EC mechanism shown in eq 3 comes from the above spectral data, as well as analysis of the current–voltage curves as a function of scan rate and temperature. The first oxidation of (TPP)Mn(NO) has a peak geometry ($E_p - E_{p/2} = 60 \pm 10$ mV) consistent with a reversible, one-electron transfer followed by a rapid chemical reaction.[26] This well-shaped oxidation peak ($E_p = +0.48$ V at a scan rate of 0.2 V/s) is not reversibly coupled to a reduction process near this potential, but rather generates two poorly separated cathodic peaks at approximately −0.2 V. These peaks at negative potentials are not present until the potential is scanned to values more positive than 0.55 V and are coupled to an anodic peak at ~−0.1 V vs. SCE. It is important to note that the two newly generated cathodic peaks correspond to potentials for the metal-centered reduction of $(TPP)MnClO_4$ and another form of (TPP)MnX, while the single anodic peak corresponds in potential to the metal-centered oxidation of (TPP)Mn to yield $[(TPP)Mn]^+$.[25] These peaks are not present upon initial cathodic scans and disappear after repeated cycling of the potential between 0.0 and −0.4 V, thus revealing these processes as due to electroactive species generated at the electrode surface and not found in the bulk of solution.

**Reduction of (TPP)Mn(NO).** The first and second reductions of (TPP)Mn(NO) remained reversible in all solvents and were shifted in a manner consistent with formation of (TPP)Mn(NO)(S) and $[(TPP)Mn(NO)(S)]^-$. Measured half-wave potentials for these processes are listed in Table I. The first reduction of (TPP)Mn(NO) occurs at −0.92 V in $CH_2Cl_2$ (peak 1, Figure 1a), which is approximately 680 mV positive of the first ring-centered reduction for (TPP)MnX in the same solvent (peak 1, Figure 1b). Although the former reduction is reversible on the cyclic voltammetric time scale, atempts to bulk generate the reduced species for spectral characterization were unsuccessful. UV–visible and ESR spectroscopy of the solutions during and after bulk electrolyses in $CH_2Cl_2$ invariably produced the spectrum typical of (TPP)Mn, thus suggesting dissociation of NO from $[(TPP)Mn(NO)]^-$ on the longer time scale of controlled-potential electrolysis. Also, cyclic voltammograms of the reduced species did not exhibit current–voltage curves of $[(TPP)Mn(NO)]^-$, but rather those of (TPP)Mn. Experiments using an optically transparent thin-layer electrode (OTTLE) resulted in the same spectral behavior as seen by bulk electrolysis experiments; again no evidence for the presence of a nitrosylated complex in solution was found after reduction had occurred.

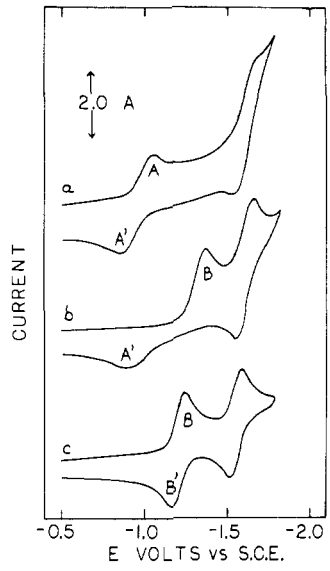


**Figure 3.** Cyclic voltammograms for $10^{-3}$ M (TPP)Mn(NO) dissolved in three solvent mixtures: (a) $CH_2Cl_2$/0.1 M TBAP; (b) $CH_2Cl_2$ containing $2 \times 10^{-3}$ M pyridine and 0.1 M TBAP; (c) pyridine/0.1 M TBAP. A, A′, B, and B′ represent the processes defined in Scheme I.

The second reduction (peak 2, Figure 1a) of (TPP)Mn(NO) occurs at −1.60 V vs. SCE in $CH_2Cl_2$/0.1 M TBAP solution, and is at an identical potential for the second reduction of (TPP)MnCl (see Figure 1). The fact that this reduction is separated from the first reduction (reaction 1) by nearly 700 mV argues against a ring-centered reduction since one would expect the potentials to be separated by 420 ± 100 mV, as is the case for most metalloporphyrins.[31] The reduction of (TPP)Mn(NO) is always reversible on the cyclic voltammetric time scale, which is not true for (TPP)MnCl. Previous studies of (TPP)MnX have shown that the reversibility of this reaction is associated with the ability of the counterion to remain coordinated after reduction, and only where $X = N_3^-$ are totally reversible waves obtained.[32] This difference in reversibility between (TPP)Mn(NO) and (TPP)MnCl suggests that NO remains coordinated (on short time scales) after the reduction shown by eq 2. The alternate possibility that NO rapidly and reversibly dissociates from $[(TPP)Mn(NO)]^-$ before further reduction at −1.60 V may be dismissed on the basis of measurements made in a number of other solvents (see later sections). For example, in $Me_2SO$ the difference in half-wave potentials between $[(TPP)Mn(NO)]^-$ and $[(TPP)Mn]^-$ reduction is 240 mV, strongly suggesting that different reacting species are present in each solution.

**Studies of (TPP)Mn(NO) in Mixed-Solvent Systems.** The electron-transfer reactions of (TPP)Mn(NO) were studied in three mixed-solvent systems: $DMF/CH_2Cl_2$, $Me_2SO/CH_2Cl_2$, and $py/CH_2Cl_2$. In all three solvent systems the bonding solvent acted as an axial ligand and coordinated to the neutral complex according to reaction 4 (L = py, DMF, $Me_2SO$). Six-coordinate complexes of the type (TPP)Mn(NO)(L) are not unexpected for low-spin Mn(II) and have been well characterized in the literature.[10-12]

$$(TPP)Mn(NO) + L \rightleftarrows (TPP)Mn(NO)(L) \quad (4)$$

Current–potential curves for the first reduction of (TPP)Mn(NO)(L) show a strong dependence upon both the donor ligand basicity and its concentration in $CH_2Cl_2$. In the absence

(29) Boucher, L. J.; Klinehamer, J. W. *Bioinorg. Chem.* **1973**, *2*, 231.
(30) Reed, C. A.; Kouba, J. K.; Grimes, C. J.; Cheung, S. K. *Inorg. Chem.* **1978**, *9*, 2666.
(31) Fuhrhop, J.-H.; Kadish, K. M.; Davis, D. G. *J. Am. Chem. Soc.* **1973**, *95*, 5140.
(32) Kelly, S. L. Ph.D. Dissertation, University of Houston, 1983.

Scheme I

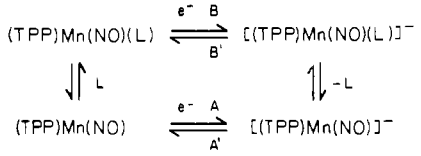


of a coordinating solvent (Figure 3a), the reduction of (TPP)Mn(NO) at −0.92 V was quasi-reversible ($\Delta E_p$ = 0.08 V at a scan rate of 100 mV/s). At low ligand to $CH_2Cl_2$ ratios, the first reduction remained quasi-reversible, but $E_{1/2}$ shifted cathodically by 60 ± 5 mV per decadic increase in ligand concentration. The magnitude and direction of this shift are consistent with loss of the bound solvent molecule upon reduction[33] (reaction 5). Finally, at higher concentrations of

$$(TPP)Mn(NO)(L) + e^- \rightleftarrows [(TPP)Mn(NO)]^- + L \quad (5)$$

binding solvent, the original reduction peak disappeared and was replaced by a new peak at more negative potentials. At the same time, the original anodic peak (labeled A′) broadened (as defined by $|E_p - E_{p/2}|$) and decreased in maximum peak current. This is shown in Figure 3b for the case of L = py.

The potential of the new cathodic peak in $CH_2Cl_2$/py mixtures (Figure 3b) was negatively shifted by 400 mV from that found in neat $CH_2Cl_2$ (Figure 3a), strongly indicating that the neutral species is coordinated by a pyridine molecule. It is important to note that the anodic peak potential (A′) shifts only slightly as a function of pyridine concentration, although the peak shape does change dramatically as a function of ligand binding. This change of anodic peak shape, as well as shifts of the cathodic peak with increased scan rate is consistent with the overall oxidation–reduction mechanism in Scheme I, where A, A′, B, and B′ represent the oxidation and reduction peaks labeled in Figure 3.

In Scheme I, dissociation of the ligand L from [(TPP)Mn(NO)(L)]⁻ slowly occurs before reoxidation (peak A′). This drawn-out oxidation process may be described as a CE mechanism where the preceding, partially rate-determining, chemical step is ligand dissociation and the following electron transfer is quasi-reversible. However, in neat pyridine the electrogenerated [(TPP)Mn(NO)(py)]⁻ is stable, and the redox process is a simple electron transfer as shown in reaction 6.

$$(TPP)Mn(NO)(py) + e^- \rightleftarrows [(TPP)Mn(NO)(py)]^- \quad (6)$$

The reversible processes in Figure 3c and reaction 6 imply that [(TPP)Mn(NO)(py)]⁻ is stable in $CH_2Cl_2$ containing high concentrations of pyridine. In this case [(TPP)Mn(NO)(py)]⁻ would be the reactant in the second reduction, and a shift in potential might be observed with increasing ligand concentration if ligand dissociation occurred upon further reduction. Unfortunately, the potentials for reduction of [(TPP)Mn(NO)(py)]⁻ in py and [(TPP)Mn(NO)]⁻ in $CH_2Cl_2$ are virtually identical, so that no shifts could be observed in $CH_2Cl_2$/py mixtures.

Finally, stability constants were calculated for addition of DMF and $Me_2SO$ to (TPP)Mn(NO) (reaction 4) using the measured shifts in half-wave potentials as a function of ligand concentration.[39] These values are log $K$ = 2.7 ± 0.1 and 3.6 ± 0.1 for DMF and $Me_2SO$, respectively. The latter value is less than 1 order of magnitude lower than that measured for $Me_2SO$ addition to (TPP)Mn (or [(TPP)MnCl]⁻) in $CH_2ClCH_2Cl$.[25]

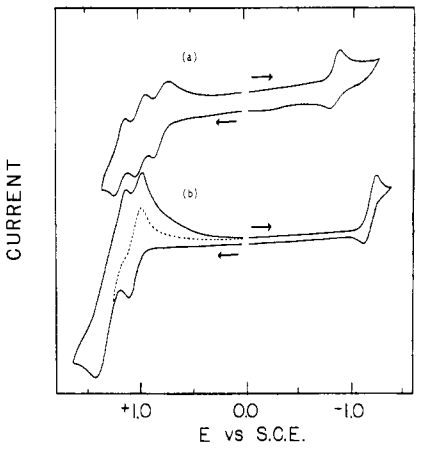


**Figure 4.** Cyclic voltammograms in $CH_2Cl_2$/0.1 M TBAP (scan rate 0.20 V/s): (a) $10^{-3}$ M (TPP)Co; (b) $10^{-3}$ M (TPP)Co(NO).

No estimates could be obtained for the addition of pyridine to (TPP)Mn(NO) as the current–potential curves do not exhibit Nernstian behavior in $CH_2Cl_2$/py mixtures. It is clear, however, that pyridine coordinates more strongly to (TPP)Mn(NO) than the oxygen donors DMF and $Me_2SO$. Only stoichiometric amounts of added pyridine are required to produce current–potential curves such as those in Figure 3b, while much higher concentrations of DMF or $Me_2SO$ were needed to produce a similar curve.

**Redox Reactions of (TPP)Co(NO) in $CH_2Cl_2$.** Figure 4 shows cyclic voltammograms of both (TPP)Co and (TPP)Co(NO) in $CH_2Cl_2$/0.1 M TBAP. The unnitrosylated complex (Figure 4a) shows three well-defined and well-separated one-electron oxidation processes. The first oxidation, which occurs at +0.79 V in $CH_2Cl_2$/0.1 M TBAP solution, was originally determined to be metal centered,[34-37] but a more recent suggestion by Scholz et al.[38] is that this reaction actually involves abstraction of an electron from the $\pi$ system of the conjugated porphyrin ring. The first reduction of (TPP)Co occurs at −0.85 V in $CH_2Cl_2$ and has been assigned as due to the Co(II)/Co(I) couple.[36,37]

As seen in Figure 4b nitrosylation of (TPP)Co leads to an increased stability of Co(II) with respect to both Co(III) and Co(I). (TPP)Co(NO) is reversibly reduced at −1.18 V (reaction 7) and reversibly oxidized at +1.01 V (reaction 8). The

$$(TPP)Co(NO) + e^- \rightleftarrows [(TPP)Co(NO)]^- \quad (7)$$

$$(TPP)Co(NO) \rightleftarrows [(TPP)Co(NO)]^+ + e^- \quad (8)$$

potentials for reaction 7 and 8 are shifted by approximately 200 mV from those for oxidation or reduction of (TPP)Co, which can be rationalized by the more stable 18-d-electron configuration of (TPP)Co(NO). A similar increased stability is also found for [(TPP)Fe(NO)]⁻, which has an 18-d-electron configuration.[9]

The electrochemically produced [(TPP)Co(NO)]⁻ is not completely stable in strongly bonding solvents and partially dissociates to give [(TPP)Co]⁻ and NO. This is illustrated in Figure 5, which shows the current–voltage curve of (TPP)Co(NO) in pyridine as a function of scan rate. At scan rates greater than 1.0 V/s the reduction is nearly reversible. However, an additional oxidation peak at $E_p \simeq -0.95$ V (at 200 mV/s) becomes increasingly more evident with decreasing

(33) Laitenen, H.; Harris, W. E. In "Chemical Analysis"; McGraw-Hill: New York, 1975; pp 227–231.
(34) Wolberg, A.; Manassen, J. *J. Am. Chem. Soc.* **1970**, *92*, 2982.
(35) Manassen, J. *Isr. J. Chem.* **1974**, *12*, 1059.
(36) Truxillo, L. A.; Davis, D. G. *Anal. Chem.* **1975**, *47*, 2260.
(37) Walker, F. A.; Beroiz, D.; Kadish, K. M. *J. Am. Chem. Soc.* **1976**, *98*, 3484.
(38) Scholz, W. F.; Reed, C. A.; Lee, Y. J.; Scheidt, W. R.; Lang, G. *J. Am. Chem. Soc.* **1982**, *104*, 6791.
(39) Kadish, K. M.; Bottomley, L. A.; Beroiz, D. *Inorg. Chem.* **1978**, *17*, 1124.

Table II. Half-Wave Potentials for the First Reduction of (TPP)Co(NO) in Selected Solvents

| solvent | $E_{1/2}$, V vs. SCE | $E_{1/2}$, V vs. $Fc^+/Fc$ | solvent | $E_{1/2}$, V vs. SCE | $E_{1/2}$, V vs. $Fc^+/Fc$ |
|---|---|---|---|---|---|
| $CH_2Cl_2$ | −1.18 | −1.67 | DMF | −0.97 | −1.50 |
| $CH_2ClCH_2Cl$ | −1.20 | −1.69 | DMA | −0.96 | −1.54 |
| PhCN | −1.15 | −1.60 | py | −1.12 | −1.63 |
| THF | −1.15 | −1.71 | | | |

Table III. Formation Constants for Axial Ligation of (TPP)Mn(NO) and $[(TPP)Co(NO)]^+$ by DMF, $Me_2SO$, and py in $CH_2Cl_2$

| species | log $K$ DMF | $Me_2SO$ | py |
|---|---|---|---|
| (TPP)Mn(NO)(L) | 2.7 ± 0.1 | 3.6 ± 0.1 | >4 |
| $[(TPP)Co(NO)(L)]^+$ | 3.1 ± 0.1 | 3.3 ± 0.1 | 5.3 ± 0.2 |

scan rates. The potential of this peak exactly matches that for $[(TPP)Co]^-$ oxidation in neat pyridine, suggesting that dissociation of NO has occurred after reduction. Similar NO dissociation is observed in PhCN, THF, and DMA and may be due to the fact that $[(TPP)Co(NO)]^-$ has an unfavorable 19-d-electron configuration.

The oxidation of (TPP)Co(NO) is also characterized by an increased lability of the NO ligand. The first oxidation is reversible only in $CH_2Cl_2$ and in this solvent yields a short-lived $[(TPP)Co(NO)]^+$ complex as shown in eq 8. The second oxidation has nearly twice the peak current of the first oxidation but has a broader peak shape ($E_p - E_{p/2} = 70$ mV at $v = 200$ mV/s) than that expected for a diffusion-controlled, two-electron transfer. Differential-pulse polarograms were carried out from 0 to +1.6 V and reveal that the second oxidation consists of two poorly separated oxidation peaks at +1.26 and + 1.38 V.

Spectra were obtained at a thin-layer optically transparent electrode after the first oxidation and were similar to that of $[(TPP)Co]^{2+}$,[34] thus suggesting that dissociation of NO and further oxidation of $[(TPP)Co]^+$ had occurred. Reversal of the potential, however, regenerated the original spectrum of (TPP)Co(NO). Attempts were also made to spectrally identify the products of the second oxidation. Although novel spectra were generated, the lack of well-defined peaks in the current–voltage curves preclude the assignment of a given spectral product to a given redox reaction.

**Electrochemistry of (TPP)Co(NO) in Bonding Solvents and in Mixed-Solvent Systems.** The oxidation and reduction of (TPP)Co(NO) were investigated in seven nonaqueous solvents. Attempts were made to obtain measurements in five other common electrochemical solvents for comparison with (TPP)Mn(NO), but due to low solubility of the complex this was not possible. A list of the solvents utilized and the measured first reduction potentials is given in Table II. A second reduction process was observed in most of the solvents, but in all cases this reaction was irreversible and located at the edge of the solvent potential limit. Potentials for this reduction

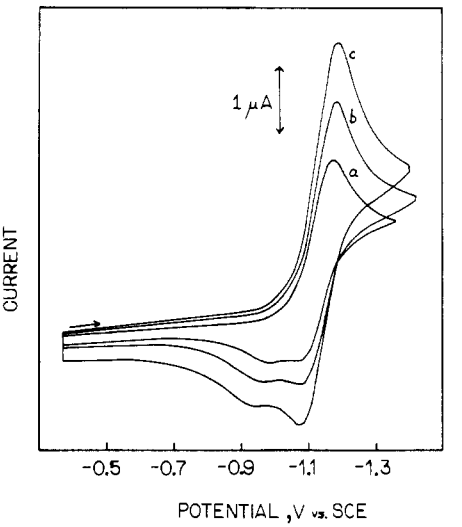


**Figure 5.** Cyclic voltammograms for the first reduction of (TPP)Co(NO) in pyridine, 0.1 M TBAP solution. Scan rates: (a) 60 mV/s; (b) 100 mV/s; (c) 200 mV/s.

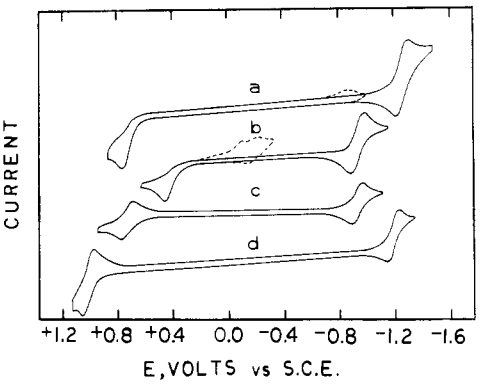


**Figure 6.** Cyclic voltammograms in $CH_2Cl_2$/0.1 M TBAP (scan rate 100 mV/s): (a) (TPP)Cr(NO); (b) (TPP)Mn(NO); (c) (TPP)Fe(NO); (d) (TPP)Co(NO). The dashed lines in parts a and b represent the rereduction of $[(TPP)M]^+$ or (TPP)MX obtained after rapid decomposition of $[(TPP)M(NO)]^+$.

were close to those for reduction of $[(TPP)Co]^-$[37] and were not investigated in this study. Oxidation potentials for (TPP)Co(NO) are also not listed in Table II since reversible reactions were obtained only in $CH_2Cl_2$ and $CH_2ClCH_2Cl$.

For the case of (TPP)Co, only small shifts are observed in the reduction half-wave potentials as a function of solvent.[36,37] This is also the case for (TPP)Co(NO), which appears to interact only slightly with the solvent. As seen in Table II, potentials for the first reduction varied by only 60 mV between the nonbonding solvent $CH_2ClCH_2Cl$ and the strongly bonding solvent pyridine. Larger shifts did occur for DMF and DMA, but as discussed below for DMF, this solvent did not bind to (TPP)Co(NO) as might be expected.

Cyclic voltammograms of (TPP)Co(NO) in $CH_2Cl_2$ containing DMF, $Me_2SO$, or pyridine suggest that there is little

Table IV. Half-Wave Potentials (V vs. SCE) for the First Reduction and First Oxidation of $(TPP)M^{II}(NO)$ and $(TPP)M^{II}$ (Where M = Cr, Mn, Fe, and Co) in $CH_2Cl_2$/0.1 M TBAP

| M | $E_{1/2}^{ox}$ (TPP)M(NO) | $E_{1/2}^{ox}$ (TPP)M | $\Delta E_{1/2}^{ox}$ [a] | $E_{1/2}^{red}$ (TPP)M(NO) | $E_{1/2}^{red}$ (TPP)M | $\Delta E_{1/2}^{red}$ [a] |
|---|---|---|---|---|---|---|
| Cr | 0.79[b,c,e] | −0.82[j] | >1.61[c] | −1.27 | ~−1.19[e] | −0.08 |
| Mn | 0.48[b,c] | −0.16[f] | >0.64[c] | −0.90 | ~−1.51[f] | +0.61 |
| Fe | 0.72[d] | 0.22[g] | 0.50 | −0.91[d] | −1.06[g] | +0.15 |
| Co | 1.01 | 0.75[h] | 0.26 | −1.18 | −0.86[i] | −0.32 |

[a] $\Delta E_{1/2} = E_{1/2}((TPP)M(NO)) - E_{1/2}((TPP)M)$. [b] $E_{pa}$ measured at 200 mV/s. [c] Reference 26. [d] Reference 8. [e] Reference 20. [f] Reference 25. [g] Bottomley, L. A.; Kadish, K. M. *Inorg. Chem.* **1981**, *20*, 1348. [h] Reference 36. [i] Reference 37. [j] $E_{pc}$ measured at 200 mV/s.

Scheme II

$$(TPP)Co(NO) + DMF \rightleftharpoons [TPP)Co(NO)(DMF)]^+ + e^-$$
$$\downarrow\uparrow DMF$$
$$[(TPP)Co(DMF)_2]^+ + NO$$

or no axial interaction between the solvent molecules and the neutral or singly reduced nitrosyl complexes. All reductions remained reversible upon addition of ligands to $CH_2Cl_2$, and only small changes were observed in the potential for reaction 7. A lack of coordination was also indicated by the electronic absorption spectra, which were invariant with additions of donor ligands.

In contrast to the invariance of redox potential for reaction 7, the half-wave potential of reaction 8 was extremely dependent upon added ligand basicity and concentration. This dependence of $E_{1/2}$ arises from the strong affinity of $[(TPP)Co(NO)]^+$ and $[(TPP)Co]^+$[39] for axial ligands. In $CH_2Cl_2$/DMF mixtures, the first oxidation remained reversible at low DMF concentrations ($10^{-3}$–$10^{-2}$ M) and exhibited a negative shift of 60 mV per decadic increase in ligand concentration. From this potential dependence, one can assume that DMF coordinates to $[(TPP)Co(NO)]^+$ but not (TPP)Co(NO) as shown in reaction 9. Estimates of the formation

$$(TPP)Co(NO) + DMF \rightleftharpoons [(TPP)Co(NO)(DMF)]^+ + e^- \quad (9)$$

constant for the addition of DMF to the oxidized species (reaction 10) were calculated from the potential shifts as a

$$[(TPP)Co(NO)]^+ + DMF \rightleftharpoons [(TPP)Co(NO)(DMF)]^+ \quad (10)$$

function of DMF concentration and yielded a value of $\log K_1 = 3.1 \pm 0.1$. This value is listed in Table III along with related formation constants for (TPP)Mn(NO).

At DMF concentrations larger than $10^{-2}$ M, the first oxidation peak was not reversibly coupled to the return reduction which occurred at significantly more negative potentials. At the same time, further oxidation peaks became better defined and two oxidations could be observed at potentials similar to those observed for (TPP)Co in $CH_2Cl_2$. This electrochemical data suggest that NO is lost upon oxidation with subsequent formation of $[(TPP)Co(DMF)_n]^+$. Previous studies[35,36,39] of (TPP)Co suggest that the oxidized product binds two DMF molecules ($n = 2$), so that replacement of NO with DMF would be the driving force of the chemical reaction following oxidation. This is shown in Scheme II.

A similar mechanism as shown in Scheme II was found to apply in $CH_2Cl_2/Me_2SO$ solvent mixtures. The stronger coordinating ability of $Me_2SO$ caused the oxidation to occur via an EC mechanism at lower ligand concentrations relative to DMF ($3 \times 10^{-3}$ M vs. $10^{-2}$ M). However, the anodic peak potential continued to shift negatively by 60 mV per decadic increase in $Me_2SO$ concentration up to 2.0 M, confirming that $Me_2SO$ coordinated to $[(TPP)Co(NO)]^+$ before displacement of NO. Estimates of a stability constant for formation of $[(TPP)Co(NO)(Me_2SO)]^+$ were calculated from shifts in $E_{pa}$ and gave a $\log K_1 = 3.3 \pm 0.1$. For the strongly coordinating pyridine, 1 equiv of added ligand induced an EC mechanism similar to the one shown in Scheme II, for the case of DMF. The first oxidation shifted negatively by 200 mV relative to that in neat $CH_2Cl_2$ solution and then underwent a negative shift of 60 mV per decadic increase in [py]. Again, as also occurred with DMF and $Me_2SO$ as ligands, the second oxidation split into two separate reactions. From the potential dependence of the first oxidation, $\log K = 5.3 \pm 0.2$ was calculated for formation of $[(TPP)Co(NO)(py)]^+$ from $[(TPP)Co(NO)]^+$. The value of $\log K_1 = 5.3$ is 10 orders of magnitude less than that for formation of $[(TPP)Co(py)_2]^+$ from $[(TPP)Co]^+$ and is the driving force for rapid displacement of the NO ligand from $[(TPP)Co(NO)(py)]^+$.

**Comparison of (TPP)M(NO) Electrochemistry (M = Cr(II), Mn(II), Fe(II), and Co(II)).** It is of some interest to compare the difference in potentials for oxidation and reduction of (TPP)M(NO) to that for (TPP)M in the presence of 0.1 M TBAP. This is done in Table IV, which lists $E_{1/2}$ or $E_{pa}$ for each reaction. As seen in this table, there is a striking stabilization of the M(II) species against the M(III) species upon NO binding, with the stabilization ($\Delta E_{1/2}^{ox}$) varying from 0.26 V for (TPP)Co(NO) to over 1.61 V for (TPP)Cr(NO). NO is known to stabilize the lower oxidation state of the central metal through $\pi$ bonding. For the complexes under investigation, the amount of stabilization follows the order Cr > Mn > Fe > Co, which reflects the proposed effect of $\pi$ bonding in the above series.[16–18] If we now consider the first reduction of (TPP)M(NO), the behavior is not straightforward. The anion $[(TPP)M(NO)]^-$ is stabilized over (TPP)M(NO) for Fe and Mn ($\Delta E_{1/2}^{red} = 0.15$ and 0.61 V), while (TPP)M(NO) is stabilized over $[(TPP)M(NO)]^-$ for Cr and Co ($\Delta E_{1/2}^{red} = -0.08$ and $-0.32$ V).

The differences in redox behavior between (TPP)Mn(NO) and (TPP)Cr(NO) on the one hand and (TPP)Fe(NO) and (TPP)Co(NO) on the other are not surprising since the number of electrons present in the (M–N–O) system dictates the nature of the (M–N–O) bond. According to the nomenclature of Enemark and Feltham,[18] (TPP)Cr(NO) and (TPP)Mn(NO) belong to the $\{MNO\}^5$ and $\{MNO\}^6$ classes, respectively, and are characterized by a linear (M–N–O) bond with *three* electrons involved, while (TPP)Fe(NO) and (TPP)Co(NO) belong to the $\{MNO\}^7$ and $\{MNO\}^8$ classes, respectively, and are characterized by a bent (M–N–O) bond, involving one or two electrons.

Analysis of the observed behavior is made easier when the effects of $\pi$ bonding from the metal ion to the nitrosyl molecule are weighed against the tendency of metal moieties to maintain a stable electron configuration, known as the EAN (effective atomic number) rule. As previously mentioned, the importance of $\pi$ bonding diminishes along the order Cr > Mn > Fe > Co, but the importance of the EAN rule to the complexes of interest follows a different trend. The reduction and oxidation of (TPP)Cr(NO), a 15-electron configuration, are governed solely by $\pi$ stabilization. Likewise, the oxidation of (TPP)Mn(NO), a 16-electron configuration, involves $\pi$-bonding effects. However, reduction of (TPP)Mn(NO) creates a more favorable 17-electron configuration, with the electron going into a bonding ($\sigma_n + d_{z^2} + d_{yz}$) orbital. Indeed, Table IV shows that the relative ease of reduction is greatest for the Mn complex, reflecting the combined effects of both stabilization mechanisms. (TPP)Fe(NO), a 17-electron configuration, experiences less $\pi$ stabilization than Cr or Mn, due to the bent (M–N–O) bond. Oxidation of this complex would produce a less desirable 16-electron configuration with the electron withdrawn from a bonding $\sigma_n$ orbital. This contributes to the increased stability of $(TPP)Fe^{II}(NO)$ toward oxidation over the nonnitrosylated complex. However, in this case, reduction produces the most favorable 18-electron configuration, with all bonding orbitals filled, and this is reflected in the relative ease of reduction of (TPP)Fe(NO). (TPP)Co(NO) has the ideal 18-electron configuration with all bonding orbitals filled, and the neutral species thus exhibits increased stability (relative to (TPP)Co) over either the reduced or oxidized species. In this complex, $\pi$ stabilization is minimal, and the EAN rule predominates over the redox reactions.

**Acknowledgment.** The support of the National Science foundation (Grant CHE-8215507) and the National Institutes of Health (Grant GM 25172) is gratefully acknowledged.

**Registry No.** (TPP)Mn(NO), 54438-77-6; (TPP)Co(NO),

42034-08-2; (TPP)Mn(NO)$^+$, 89321-11-9; (TPP)Mn(NO)$^-$, 89302-22-7; (TPP)Mn(NO)$^{2-}$, 89302-23-8; (TPP)Co(NO)$^-$, 89302-24-9; (TPP)Mn(NO)(DMF), 89320-98-9; (TPP)Mn(NO)($Me_2SO$), 89302-25-0; (TPP)Mn(NO)(py), 89302-26-1; [(TPP)Co(NO)(DMF)]$^+$, 89302-27-2; [(TPP)Co(NO)($Me_2SO$)]$^+$, 89302-28-3; [(TPP)Co(NO)(py)]$^+$, 89302-29-4; [(TPP)Cr(NO)]$^+$, 89302-30-7; (TPP)Cr, 58344-06-2; [(TPP)Fe(NO)]$^+$, 70622-46-7; (TPP)Fe, 16591-56-3; [(TPP)Mn]$^+$, 59388-92-0; [(TPP)Cr]$^+$, 63692-18-2.

Contribution from the Department of Chemistry,
North Carolina State University, Raleigh, North Carolina 27650

# Mössbauer and Raman Spectroscopic Studies of Substituted Pyridinium Bromoantimonate(III) Compounds

SHEILA W. HEDGES and L. H. BOWEN*

*Received July 26, 1983*

A series of substituted pyridinium bromoantimonate(III) compounds with anions $SbBr_4^-$, $SbBr_5^{2-}$, and $Sb_2Br_9^{3-}$ have been prepared and studied by Raman and $^{121}Sb$ Mössbauer spectroscopies. The Mössbauer spectra yield two main diagnostic parameters: the isomer shift and the quadrupole coupling constant. The general trend from $SbBr_3$ to $SbBr_5^{2-}$ is a decrease in both these parameters as the number of bromines surrounding the antimony increases. The isomer shift (relative to InSb) ranges from −7.64 to −8.20 mm/s for the $SbBr_4^-$ anion, from −8.90 to −9.01 mm/s for $Sb_2Br_9^{3-}$, and from −8.20 to −9.33 mm/s for $SbBr_5^{2-}$. The quadrupole coupling constant ranges from +5.9 to +8.0 mm/s for $SbBr_4^-$ and from 0 to +5.2 mm/s for the $Sb_2Br_9^{3-}$ and $SbBr_5^{2-}$ anions. Substitution on the pyridinium ring has a significant effect on the Mössbauer parameters of a given anion, probably due to distortion of the anion geometry. Raman spectra obtained for these compounds are discussed in relation to assignments in the literature. The spectra show a surprisingly large variation in the region below 300 $cm^{-1}$, even between compounds with the same stoichiometry. The region between 1000 and 300 $cm^{-1}$ is not particularly sensitive to the stoichiometry. Two of the strongest low-frequency bands, one in the region around 150 $cm^{-1}$ and one in the region 60–30 $cm^{-1}$, exhibit distinct correlation with the changes in isomer shift as the cation is varied.

## Introduction

The reaction of antimony tribromide with amine hydrobromides yields a large variety of types of compounds. Both aliphatic and aromatic amines have been used in studies of the various factors that influence the stoichiometry and structure of such compounds. For example, the various pyridinium bromoantimonates have been studied by vibrational spectroscopy,[1,2] TGA and DTA,[3] X-ray diffraction,[4-9] NMR,[10] and Mössbauer spectroscopy.[11-14] Although several metal ion, ammonium, and pyridinium bromoantimonates of various stoichiometries have been studied by Mössbauer spectroscopy, only two substituted pyridinium bromoantimonate(III) compounds have been reported.[11,12] We selected a group of substituted pyridinium bromoantimonate(III) compounds to investigate the effect of cation ring substitution on the anion using Raman and Mössbauer spectroscopies. Compounds of three different stoichiometries were examined: $RSbBr_4$ (R = pyH, 2-MepyH, 3-MepyH, 4-MepyH, 2,4,6-$Me_3$pyH, 2-Br(py)H, 2-Cl(py)H), $R_2SbBr_5$ (R = 3-MepyH, 4-MepyH, 2-Br(py)H, 3-COOHpyH), and $R_3Sb_2Br_9$ (R = 2,4-$Me_2$pyH, 2,4,6-$Me_3$pyH). The results are discussed in terms of known and likely structures of the complex Sb(III) species.

## Experimental Section

The compounds $RSbBr_4$, $R_2SbBr_5$, and $R_3Sb_2Br_9$ were prepared by slight variations in the method described by Whealey and Yeakley[15] and by Stewart et al.[16] Antimony(III) bromide solution was prepared by dissolving $Sb_2O_3$ in hot hydrobromic acid (48% HBr). To this solution was added a stoichiometric amount of the appropriate amine dissolved in cold hydrobromic acid. The reaction mixture was then heated to dissolve any solids and set aside to cool slowly. For most of these amines, the compound obtained depends on the experimental conditions[2] such as concentration of reactants and particularly the solvent. When mixtures of compounds with different stoichiometries were obtained, they could usually be separated by recrystallization. Recrystallization, when necessary, was done either from hot aqueous hydrobromic acid or from acetone/HBr mixed solvent. All samples were analyzed for Sb and those that were recrystallized from acetone were also analyzed for C and H. In some cases, successive recrystallizations were needed until the material gave the appropriate elemental analysis. No sample was used for further experiments until the elemental analyses were in good agreement with theoretical values.

(1) Allen, G. C.; McMeeking, R. F. *Inorg. Chim. Acta* **1977**, *23*, 185–90.
(2) Leroy, M. J. F.; Goetz, G. J. *Bull. Soc. Chim. Fr.* **1979**, 120–3.
(3) Jha, N. K.; Rizvi, S. S. A. *J. Inorg. Nucl. Chem.* **1974**, *36*, 1479–89.
(4) Porter, S. K.; Jacobson, R. A. *J. Chem. Soc. A* **1970**, 1359–62.
(5) DeHaven, P. W.; Jacobson, R. A. *Cryst. Struct. Commun.* **1976**, *5*, 31–4.
(6) Carola, J. M.; Freedman, D. D.; McLaughlin, K. L.; Reim, P. C.; Schmidt, W. J.; Haas, R. G.; Broome, W. J.; DeCarlo, E. A.; Lawton, S. L. *Cryst. Struct. Commun.* **1976**, *5*, 393–9.
(7) Lawton, S. L.; Jacobson, R. A. *Inorg. Chem.* **1968**, *7*, 2124–34.
(8) Lawton, S. L.; Hoh, D. M.; Johnson, R. C.; Knisely, A. S. *Inorg. Chem.* **1973**, *12*, 277–83.
(9) Lawton, S. L.; Jacobson, R. A.; Frye, R. S. *Inorg. Chem.* **1971**, *10*, 701–8.
(10) Kidd, R. G.; Mathews, R. W. *J. Inorg. Nucl. Chem.* **1975**, *37*, 661–3.
(11) Donaldson, J. D.; Southern, J. T.; Tricker, M. J. *J. Chem. Soc., Dalton Trans.* **1972**, 2637–9.
(12) Alamgir, M.; Barnard, P. W. C.; Donaldson, J. D. *J. Chem. Soc., Dalton Trans.* **1980**, 1542–4.
(13) Donaldson, J. D.; Thomas, M. J. K. *Inorg. Nucl. Chem. Lett.* **1978**, *14*, 93–5.
(14) Ballard, J. G.; Birchall, T.; Milne, J. B.; Moffett, W. D. *Can. J. Chem.* **1974**, *52*, 2375–9.
(15) Whealey, R. D.; Yeakley, R. L. *J. Inorg. Nucl. Chem.* **1963**, *25*, 365–8.
(16) Stewart, J. M.; MchLaughlin, K. L.; Rossiter, J. J.; Hurst, J. R.; Haas, R. G.; Rose, V. J.; Ciric, B. E.; Murphy, J. A.; Lawton, S. L. *Inorg. Chem.* **1974**, *13*, 2767–9.

0020-1669/84/1323-1458$01.50/0 